Constructing cation defects through selective etching tetrahedral sites in Co_3O_4 for enhanced oxygen evolution reaction

Xiaotian Wu,[a] Qian Zhu, [a] Yingge Cong,[c] Zhibin Geng, [a] Keke Huang, [a] Mei Han, [*a], and Zhiyu Shao[*a,b]

Experimental Section

Chemicals and reagents

$Co(NO_3)_2·6H_2O$, $Zn(NO_3)_2·6H_2O$ and NaOH were purchased from Sinopharm Chemical Reagent Co. Ltd (Shanghai, China) and of analytical grade purity. Methanol was purchased from Sinopharm Chemical Reagent Co. Ltd (Shanghai, China) and was Guaranteed Reagent. 2-Methylimidazole was purchased from Aladdin and the purity was 98%. Cetyltrimethylammonium bromide (CTAB) was purchased from Aladdin and the purity was 99%.

Synthesis of samples

The required samples were synthesized using the method reported in the literature and appropriate improvements were made.[1,2] Specifically, $Co(NO_3)_2·6H_2O$, $Zn(NO_3)_2·6H_2O$ and 5 mg of CTAB were dissolved in 10 mL of deionized water as Solution A, with the total amount of metal ions Co and Zn maintained at 1 mmol. 4.54 g of 2-methylimidazole was dissolved in 70 mL of deionized water as Solution B. Then quickly pour Solution A into Solution B under continuous stirring and purple precipitates were immediately generated. Continue stirring at room temperature for 30 min and age for 24 h. The purple solid was centrifuged, washed with water and methanol and dried at 60 °C. The obtained powder was then calcined at 550 °C for 2 h with a ramp rate of 2 °C/min. The molar ratios of Co and Zn in Zn-Co_3O_4-50:1, Zn-Co_3O_4-20:1 and Zn-Co_3O_4 are 50:1, 20:1 and 5:1, respectively. The pristine Co_3O_4 was synthesized using the same method for contrast.

Zn-Co_3O_4 was immersed in concentrated NaOH solution for 5, 20 and 40 min, and the products were named Zn-Co_3O_4-5min, Zn-Co_3O_4-20min and Zn-Co_3O_4-40min, respectively. The samples impregnated with alkaline concentrations of 5 M, 10 M and 15 M were represented as V_{Zn}-Co_3O_4-5M, V_{Zn}-Co_3O_4-10M and V_{Zn}-Co_3O_4-15M, respectively. Ultrasonic dispersion was performed during the processing to ensure sufficient contact between the solid and NaOH solution. Finally, centrifugate immediately, collect the upper clear liquid additionally, wash several times with deionized water and methanol, and dry it at 60 °C.

Catalyst characterization

Powder X-ray diffraction (XRD) data was obtained by using a Rigaku D/Max 2550 diffractometer with Cu-K_α radiation testing at 40 kV and 200 mA by step scanning in the angel range of 10° to 80°. Scanning electron microscopy (SEM) images were taken with a Helios NanoLab 600I microscope operating at 10 kV, equipped with an EDS detector. Transmission electron microscopy (TEM) morphology and high-resolution TEM (HRTEM) images were collected with FEI Tecnai G2 S-Twin F20 Microscope. X-ray photoelectron spectra (XPS) were recorded with an ESCALAB 250Xi electron energy spectrometer (Thermo Fisher Scientific) and use of Al K_α (1486.6 eV) as the X-ray

excitation source. Raman spectra of catalysts were received on a RenishawinVia Confocal excited with a 532 nm wavelength laser. X-ray absorption spectra (XAS, included EXAFS and XANES) were measured at the beamline BL14W1 of SSRF (Shanghai Synchrotron Radiation Facility) in China.

Electrochemical Measurements

5 mg of catalyst and 10 μL of 5 wt % Nafion solution were dispersed in 350 μL of 2.5:1 V/V ethanol/water mixed solvent by at least 30 min sonication to form a homogeneous ink. Then 3 μL of the catalyst ink was loaded onto a glassy carbon electrode of 3 mm in diameter. Linear sweep voltammetry (LSV) and cyclic voltammetry (CV) were conducted with a CHI 760 D potentiost in a three-electrode electrochemical cell using saturated Hg/HgO electrode as the reference electrode, a Pt rod as the counter electrode, and the sample modified glassy carbon electrode as the working electrode. The electrolyte was saturated with oxygen by bubbling O_2 before the start of each experiment. The working electrode was cycled at least 10 times before data were recorded at a scan rate of 1 mV s^{-1}. The OER tests of the electrocatalysts were executed in the O_2-saturated 1 M KOH electrolyte. Electrochemical impedance spectroscopy (EIS) was also carried out and recorded at 0.65 V versus Hg/HgO with frequencies ranging from 100 kHz to 0.1 Hz under an AC voltage of 5 mV. The electrochemically active surface area (ECSA) was evaluated based on the double layer capacitance (C_{dl}) in the non-Faradaic potential region. Specifically, the samples were tested via CV measurements at various scan rates (40, 60, 80, 100 and 120 mV s^{-1}). The ECSA was calculated using the formula: ECSA = $S_c \times C_{dl}/C_s$, where S_c is the geometric area of the GC electrode, C_{dl} represents the electrochemical double-layer capacitance, and C_s denotes the specific electrochemical double-layer capacitance of the smooth surface substrate. The specific capacitance of the smooth surface (C_s) of the catalyst at the electrode was considered to be 0.1 mF cm^{-1}.

Density Functional Theory Calculations

The density function calculations were performed using Vienna ab initio simulation package (VASP) with the projector augmented-wave (PAW) method.[3,4] The generalized gradient approximation (GGA) functional parametrized by Perde Burke-Ernzerh of (PBE) was employed to describe the exchange correlation potential.[5] A plane-wave energy cutoff of 400 eV was used and the energies and forces on each atom were converged to 10-4 eV and 0.05 eV/Å, respectively. A gamma-only point was used for the Brillouin zone integrations in geometry optimization, while other calculations employed a Γ-centered K-point mesh of 3×3×2.

To build pristine Co_3O_4, Co_3O_4 (311) surface was cleaved. On the basis of pristine Co_3O_4, two tetrahedral Co units on the surface were replaced by Zn atoms to simulate the spatial situation of Zn-Co_3O_4. For V_{Zn}-Co_3O_4, one tetrahedral Zn site was removed. A vacuum layer of 1.5 nm was used along the c direction normal to the surface to avoid periodic interactions in all models. The free energies are calculated from total energy as:

$$\Delta G = \Delta E + \Delta ZPE - T\Delta S$$

where ΔE is the reaction energy, ΔZPE is the change of zero-point energy, T (298.15 K) is the temperature, ΔS is the difference in entropy.[6]

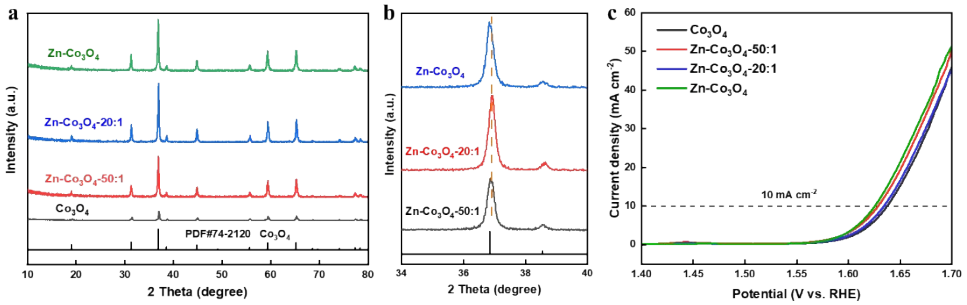

Fig. S1 (a) The XRD patterns of Co_3O_4, Zn-Co_3O_4-50:1, Zn-Co_3O_4-20:1 and Zn-Co_3O_4. (b) The XRD patterns of expanded regions of 2θ = 34-40°. (c) LSV curves of Co_3O_4, Zn-Co_3O_4-50:1, Zn-Co_3O_4-20:1 and Zn-Co_3O_4.

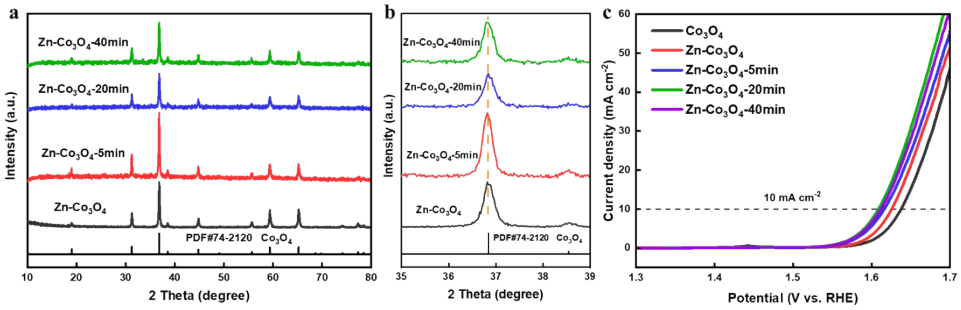

Fig. S2 (a) The XRD patterns of Zn-Co_3O_4, Zn-Co_3O_4-5min, Zn-Co_3O_4-20min and Zn-Co_3O_4-40min. (b) The XRD patterns of expanded regions of 2θ = 35-39°. (c) LSV curves of Co_3O_4, Zn-Co_3O_4, Zn-Co_3O_4-5min, Zn-Co_3O_4-20min and Zn-Co_3O_4-40min.

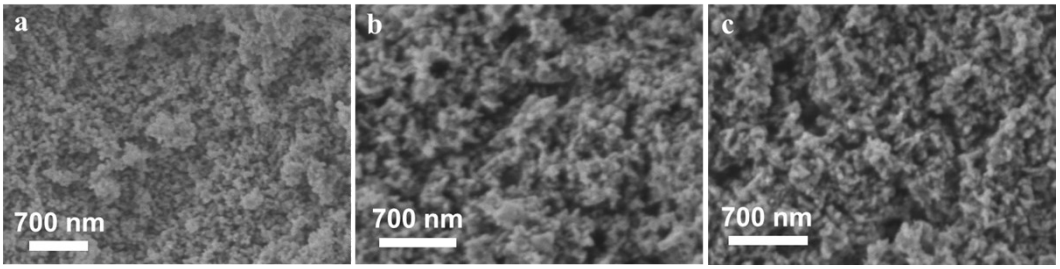

Fig. S3 SEM images of (a) Co_3O_4, (b) V_{Zn}-Co_3O_4-5M and (c) V_{Zn}-Co_3O_4-15M.

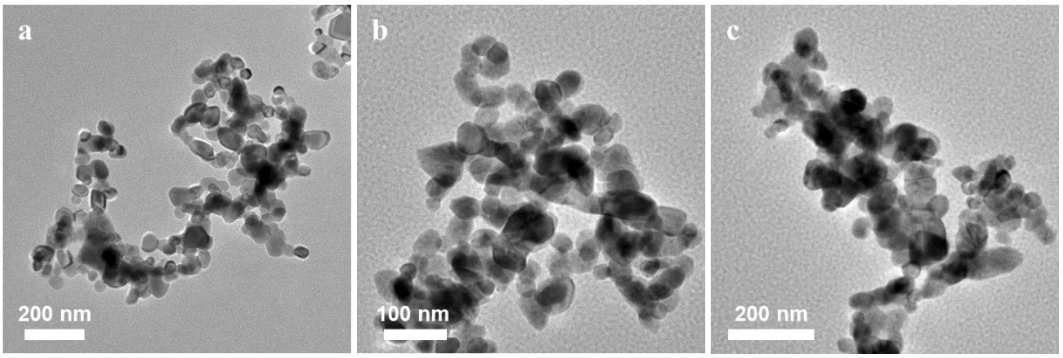

Fig. S4 TEM images of (a) Co_3O_4, (b) V_{Zn}-Co_3O_4-5M and (c) V_{Zn}-Co_3O_4-15M.

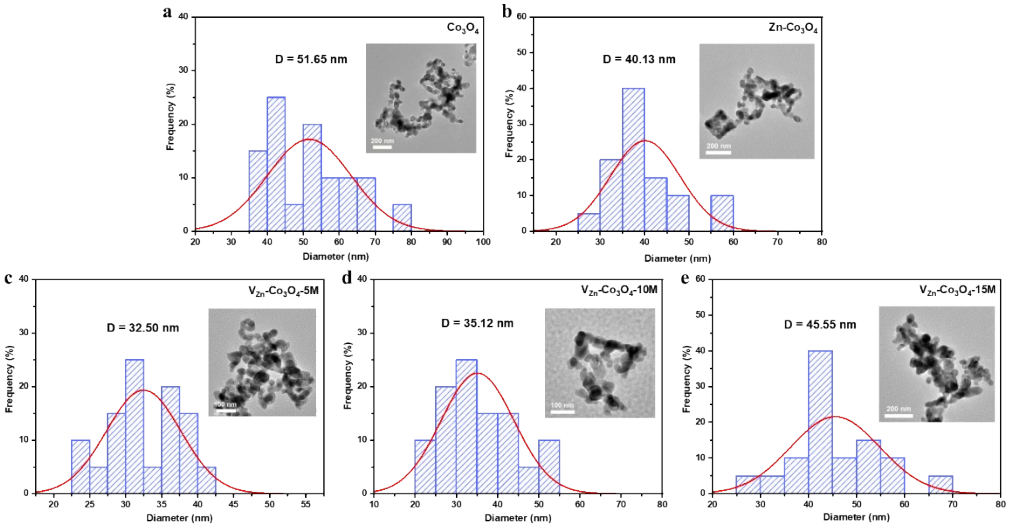

Fig. S5 TEM images and the particle size statistics of (a) Co_3O_4, (b) Zn-Co_3O_4, (c) V_{Zn}-Co_3O_4-5M, (d) V_{Zn}-Co_3O_4-10M and (e) V_{Zn}-Co_3O_4-15M.

Table S1 The parameters of particle size statistics from the TEM.

Samples	Mean particle size (nm)
Co_3O_4	51.65
Zn-Co_3O_4	40.13
V_{Zn}-Co_3O_4-5M	32.50
V_{Zn}-Co_3O_4-10M	35.12
V_{Zn}-Co_3O_4-15M	45.55

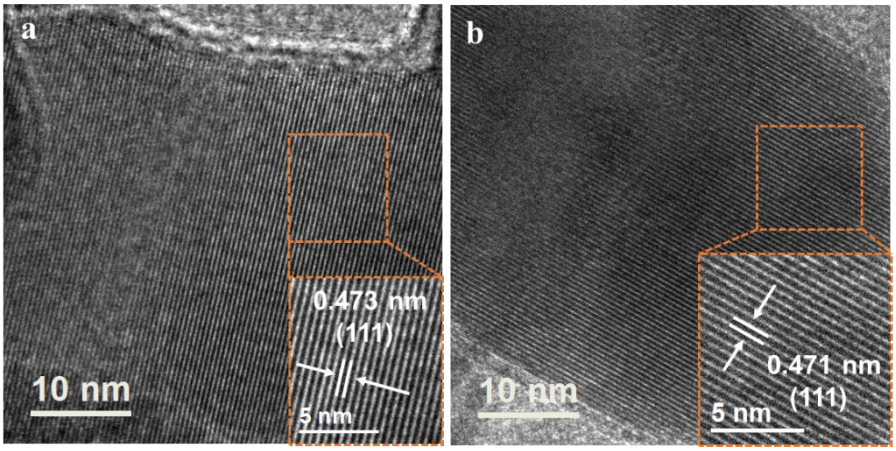

Fig. S6 HRTEM images of (a) V_{Zn}-Co_3O_4-5M and (b) V_{Zn}-Co_3O_4-15M.

Table S2 The ICP results of the upper clear liquid after processing.

Samples	Co concentration (ppm)	Zn concentration (ppm)	Actual ratio (Co/Zn)
V_{Zn}-Co_3O_4-5M	0.0056	0.0875	0.0640
V_{Zn}-Co_3O_4-10M	0.0091	0.1520	0.0599
V_{Zn}-Co_3O_4-15M	0.0266	0.1474	0.1805

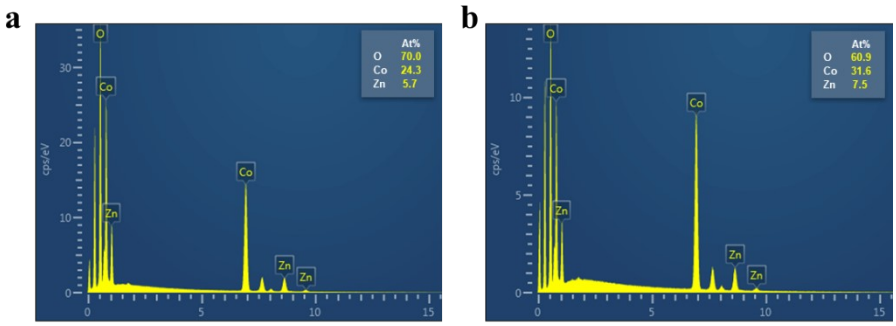

Fig. S7 The EDS results of (a) V_{Zn}-Co_3O_4-5M and (b) V_{Zn}-Co_3O_4-15M.

Table S3 The detailed EDS results of the samples.

Samples	Co At%	Zn At%	Co/Zn
Zn-Co_3O_4	24.7	5.9	4.19
V_{Zn}-Co_3O_4-5M	24.3	5.7	4.26
V_{Zn}-Co_3O_4-10M	25.3	5.4	4.69
V_{Zn}-Co_3O_4-15M	31.6	7.5	4.21

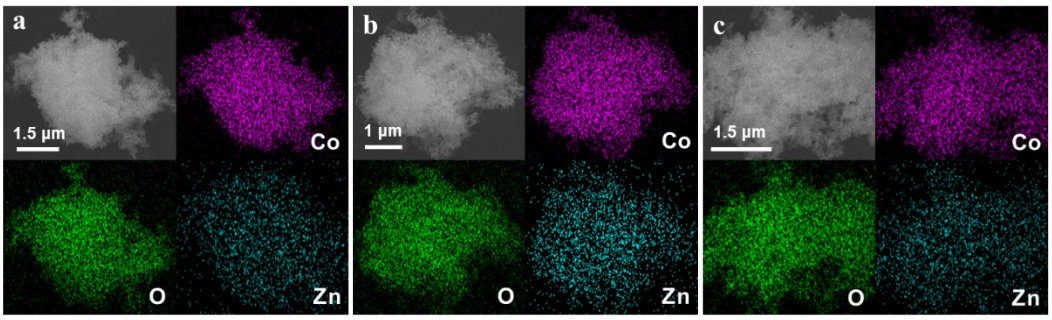

Fig. S8 The EDS elemental mapping of (a) Zn-Co_3O_4, (b) V_{Zn}-Co_3O_4-5M and (c) V_{Zn}-Co_3O_4-15M.

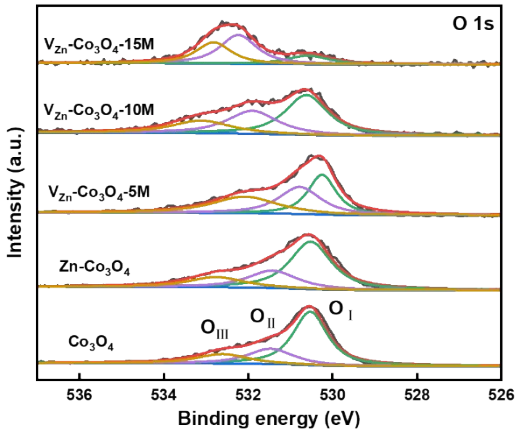

Fig. S9 The XPS spectrum of O 1s for the samples.

Table S4 The R_s and R_{ct} values of the samples at 1.574 V vs. RHE.

Samples	R_s	R_{ct}
Co_3O_4	9.642	196.7
Zn-Co_3O_4	11.47	180.7
V_{Zn}-Co_3O_4-5M	11.92	122.0
V_{Zn}-Co_3O_4-10M	11.42	48.26
V_{Zn}-Co_3O_4-15M	12.87	204.5

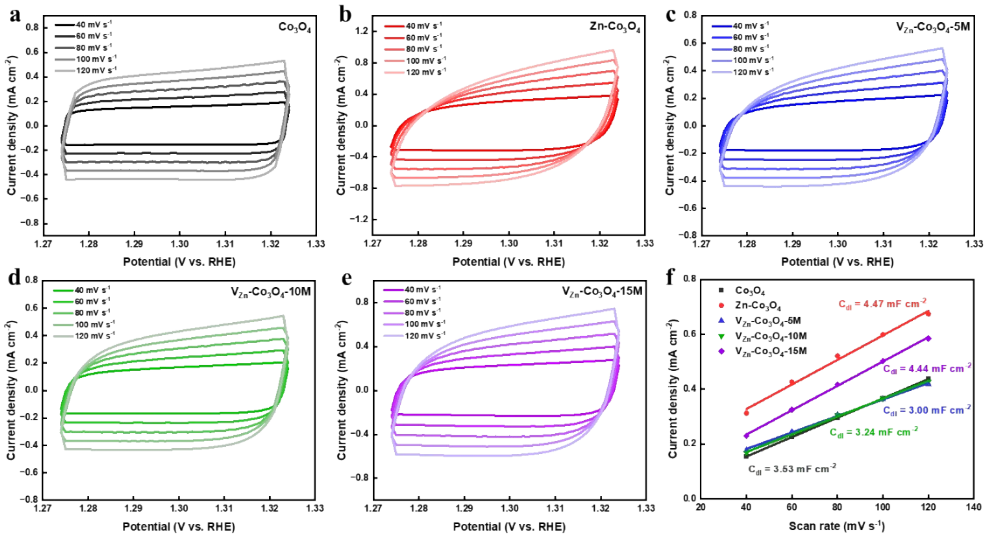

Fig. S10 CV measurements at different scan rates of (a) Co_3O_4, (b) Zn-Co_3O_4, (c) V_{Zn}-Co_3O_4-5M, (d) V_{Zn}-Co_3O_4-10M and (e) V_{Zn}-Co_3O_4-15M. (f) Current density at 1.30 V at different scan rates for the calculation of double-layer capacitance (C_{dl}).

Table S5 The C_{dl} and ECSA values.

Samples	C_{dl} (mF cm^{-2})	ECSA (cm^2)
Co_3O_4	3.53	2.50
Zn-Co_3O_4	4.47	3.16
V_{Zn}-Co_3O_4-5M	3.00	2.12
V_{Zn}-Co_3O_4-10M	3.24	2.29
V_{Zn}-Co_3O_4-15M	4.44	3.14

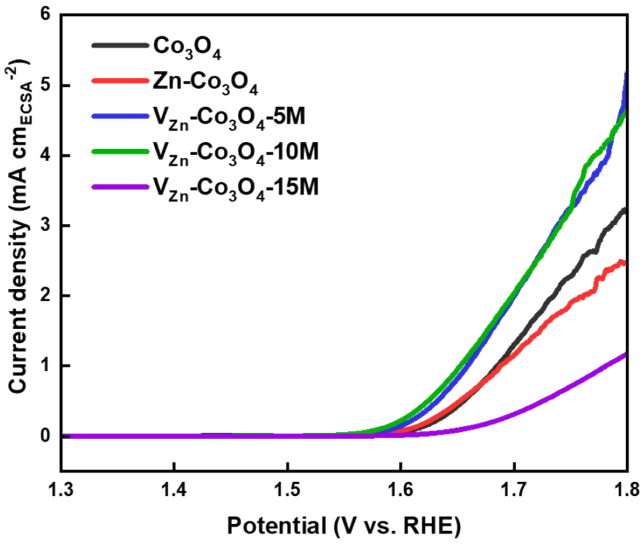

Fig. S11 LSV curves of catalysts using ECSA-normalized current density.

Table S6 A comparison of OER activity of our work with recently reported electrocatalysts.

Catalysts	Current density ($mA\ cm^{-2}$)	Overpotential (mV)	Electrolyte	References
V_{Zn}-Co_3O_4-10M	10	379	1 M KOH	**This work**
Co_3O_4/CoO	10	463	1 M KOH	[7]
Co_3O_4/SnO_2	10	487	1 M KOH	[8]
$MnCo_2O_4$	10	400	1 M KOH	[9]
PdO@Co_3O_4	10	389	1 M KOH	[10]
$Ni_{0.7}Co_{0.3}O_x$	10	394	1 M KOH	[11]
W-Co_3O_4	10	≈390	1 M KOH	[12]

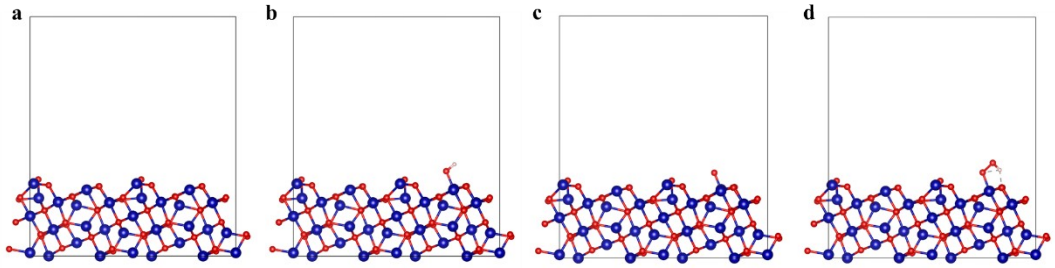

Fig. S12 (a) The optimized configurations of the substrate. The optimized configurations of (b) OH*, (c) O* and (d) OOH* intermediates on Co_3O_4.

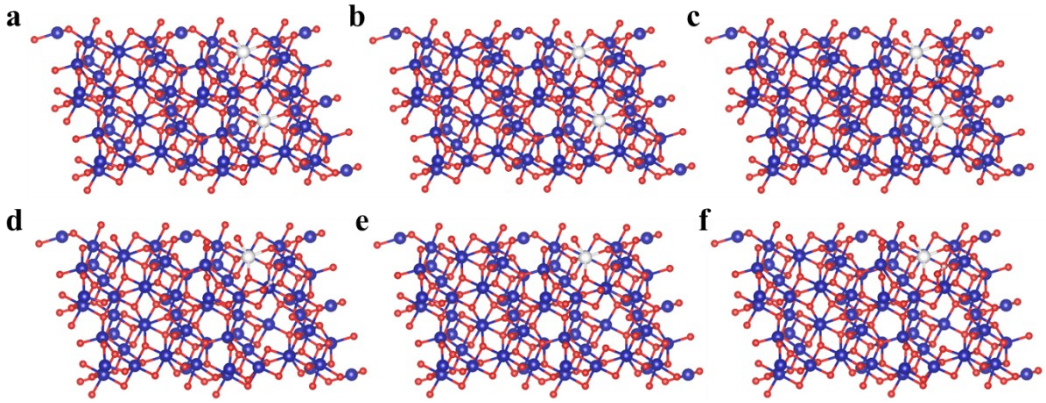

Fig. S13 The optimized configurations of (a) OH*, (b) O* and (c) OOH* intermediates on Zn-Co_3O_4. The optimized configurations of (d) OH*, (e) O* and (f) OOH* intermediates on V_{Zn}-Co_3O_4.

References

1 Y. Zhang, S. Zhang, H. Li, Y. Lin, M. Yuan, C. Nan and C. Chen, *Nano Lett.*, 2023, **23**, 9119−9125.
2 L. Zhang, Z. Jin and N. Tsubaki, *ACS Appl. Mater. Interfaces*, 2021, **13**, 50996−51007.
3 S. Nosé, *J. Chem. Phys.*, 1984, **81**, 511-519.
4 G. Kresse and D. Joubert, *Phys. Rev., B Condens. Matter*, 1999, **59**, 1758-1775.
5 B. A. Ivanov and E. V. Tartakovskaya, *Phys. Rev. Lett.*, 1997, **77**, 386.
6 Z. Gao, J. Liu, X. Chen, X. Zheng, J. Mao, H. Liu, T. Ma, L. Li, W. Wang and X. Du, *Adv. Mater.*, 2019, **31**, 1804769.
7 R. A. E. Acedera, G. Gupta, M. Mamlouk and M. D. L. Balela, *J. Alloys Compd.*, 2020, **836**, 154919.
8 J. Milikić, S. Knežević, M. Ognjanović, D. Stanković, L. Rakočević and B. Šljukić, *Int. J. Hydrogen Energy*, 2023, **48**, 27568-27581.
9 S. Natarajan, S. Anantharaj, R. J. Tayade, H. C. Bajaj and S. Kundu, *Dalton Trans.*, 2017, **46**, 14382.
10 G. S. Rocha, A. L. Silva, L. P. C. Silva, F. B. Passos and N. M. F. Carvalho, *Energy Fuels*, 2022, **36**, 12719−12728.
11 J. Chi, H. Yu, G. Li, L. Fu, J. Jia, X. Gao, B. Yi and Z. Shao, *RSC Adv.*, 2016, **6**, 90397.
12 T. Tran-Phu, M. Chatti, J. Leverett, T. K. A. Nguyen, D. Simondson, D. A Hoogeveen, A. Kiy, T. Duong, B. Johannessen, J. Meilak, P. Kluth, R. Amal, A. N. Simonov, R. K. Hocking, R. Daiyan and A. Tricoli, *Small*, 2023, **19**, 2208074.